# Investigating the relationships between peristaltic contraction and fluid transport in the human colon using Smoothed Particle Hydrodynamics

M.D. Sinnott[1*], P.W. Cleary[1], J. W. Arkwright[2] and P.G. Dinning[3]

[1] CSIRO Mathematics, Informatics and Statistics, Clayton, VIC, Australia

[2] CSIRO Materials Science and Engineering, Lindfield, NSW, Australia

[3] Department of Human Physiology & Centre for Neuroscience, Flinders University, Adelaide, SA, Australia

*Corresponding Author: Email: matthew.sinnott@csiro.au; Tel/Fax: +61 3 9545 8034 / +61 3 9545 8080

**Abstract**

Complex relationships exist between gut contractility and the flow of digesta. We propose here a Smoothed Particle Hydrodynamics model coupling the flow of luminal content and wall flexure to help investigate these relationships. The model indicates that a zone of muscular relaxation preceding the contraction is an important element for transport. Low pressures in this zone generate positive thrust for low viscosity content. The viscosity of luminal content controls the localization of the flow and the magnitude of the radial pressure gradient and together with contraction amplitude they control the transport rate. For high viscosity content, high lumen occlusion is required for effective propulsion.

**Keywords:**

Gastrointestinal Motility, Smoothed Particle Hydrodynamics, Descending Inhibition, Computational Fluid Dynamics, Peristalsis

## 1 Introduction

The gastrointestinal tract comprises of several distinct organs in sequence, extending over 7 meters in the human abdomen. Controlled propulsion and mixing of content along the digestive tract is essential for a normal life. This is achieved by a rich assortment of motor patterns that ensure that movements and propulsion are appropriate for the breakdown of food, absorption of nutrients and excretion of waste. These movements (motility) are due to coordinated contractions and relaxations of circular and longitudinal smooth muscle layers. In terms of quantitative descriptions, gut motility is one of the most complex functions in the body and when abnormalities occur there can be serious consequences. At times there are obvious causes for these abnormalities, for example tumors can impair flow and their surgical and/or radiation treatment can cause damage to the surrounding tissue, muscle and nerves with further implications for modified transport. There are, however, a host of other gastrointestinal abnormalities where the cause of abnormal intestinal transport is less clear. These functional gastrointestinal disorders (FGID) include dysphagia (difficulty in swallowing), fecal incontinence and constipation. While these are generally not life threatening they can be chronic conditions that cause major economic and social burdens because of their prevalence in society and their dramatic impact upon quality of life. In Australia around one third of the population has one or more FGID and 60% of these will seek medical attention [1].

For oesophageal FGIDs the combined technical advances in recording abnormal contractility, via oesophageal manometry, and relating these abnormalities to impaired flow [2] has seen a dramatic improvement in our understanding of the problem and therefore our ability to treat the patient. However, this is not the case for FGIDs in regions below the stomach. The small and large intestines are relatively inaccessible and obtaining detailed manometric recordings and visualizing the movement of digesta is difficult. As a result our understanding of normal pressure/flow relationships is still relatively simplistic [3]. Therefore while abnormal contractility is implicated in FGIDs [4-6], how these abnormalities relate to impaired flow remains largely unknown.

Computational modeling of gastrointestinal systems has the potential to help understand these complex relationships. Many mathematical models of peristaltic pumping in flexible tubes have been developed over the last decades and the reader is referred to [7, 8] for comprehensive reviews of

this research. The vast majority of these models do not take into account the solid wall mechanics of the flexible tube in predicting the transient wall deformation. Instead the wall shape is fully prescribed. Some exceptions to this include Carew and Pedley [9] who developed a model of peristaltic flow in the ureter with an active contracting wall coupled to the internal resistance from the intra-luminal pressures in an infinitely long tube. Such models are based on lubrication theory and are therefore limited to simple geometry systems with low inertial flows and long waves. They are well suited to studying the dynamics of the ureter. However, the development of intestinal flow models for studying the effect of single and multiple wave trains on transport requires an active wall model that can accommodate more realistic geometry and non-linear wall mechanics.

More recently detailed computational models of oesophageal motility [10, 11] have helped to define relationships between motility and flow. In addition CFD models have started to consider the effect of peristaltic motor patterns in the small intestine [12] and the stomach [13, 14]. While these studies in the stomach and small bowel have sourced anatomically accurate wall geometries from MRI, they have not attempted a 2-way coupling of the motor activity in the wall with the fluid content. Instead motor patterns are prescribed as a sequence of fixed geometric changes to the boundary. Physiologically realistic intestinal models need to be able to incorporate a number of factors such as the widely accepted law of the intestine [15] which states that a bolus moves in the digestive tract due to the combined ascending excitatory input upstream causing a contraction coupled with descending inhibitory input or Descending Inhibition (DI) causing the segment of gut immediately ahead of the bolus to relax [16, 17].

We propose a model for the coupled wall flexure and flow dynamics inside the colon subject to peristaltic waves of contraction and relaxation using the Smoothed Particle Hydrodynamics (SPH) method [18, 19]. SPH is a particle-based, transient, Lagrangian method. Computations are performed on a set of SPH ‘particles’ which move with any flow carrying local state information with them. The mesh free nature of SPH means large deformations can be modeled without requiring expensive and diffusive re-meshing. Coupling of fluid/solid motion and wall deformation is therefore captured naturally. These advantages have lead to the modeling of pulsatile blood flow in a carotid

artery bifurcation [20] and the prediction of blood flow through a non-pulsatile, axial, heart pump [21].

This colon model consists of a flexible visco-elastic cylindrical tube filled with a viscous fluid. In this initial work the intra-luminal content will be assumed to be Newtonian. The boundary model will incorporate radial contractions of the circular muscle. The addition of the longitudinal contractions of the smooth muscle will be incorporated in a future extension. The model will be used to investigate relationships between wall deformation, intra-luminal pressure and flow. We also explore the role of the DI in generating effective fluid transport. The model will then be used to determine the influence of fecal viscosity, lumen occlusion and length of contraction on transport. This model represents the first step in developing a tool to help us interpret how pressure signals recorded from manometric recordings may relate to the propulsion and mixing of intra-luminal content and how abnormalities in these pressure signals may be associated with impaired flow.

## 2 Computational model of colon and travelling peristaltic waves

Smoothed Particle Hydrodynamics (SPH) is a well established numerical method for modeling fluid dynamics. For a detailed introduction to the method, the reader is referred to Monaghan [18]. Here we give a brief summary of the method. A suitable form of the SPH continuity equation gives the evolution of the density $\rho_a$ of particle *a,* as:

$$\frac{d\rho_a}{dt} = \sum_b m_b(\mathbf{v}_a - \mathbf{v}_b) \bullet \nabla W_{ab} \qquad (1)$$

where $\mathbf{v}_a$ is the velocity and $m_b$ is the mass of particle *b*. The position vector between particles *b* and *a* is denoted as $\mathbf{r}_{ab}=\mathbf{r}_a-\mathbf{r}_b$. The value of the interpolation kernel with smoothing length *h* evaluated for the distance $|\mathbf{r}_{ab}|$ is $W_{ab} = W(\mathbf{r}_{ab},h)$. This form of the continuity equation is very effective for modeling free surfaces and has good numerical conservation properties.

In this initial model, we make the assumption that the fecal matter behaves in a Newtonian manner. This is not unreasonable as the strain rates in the bowel are low, so one would not expect shear thinning or power law behaviour. In the absence of information to the contrary a linear relationship between stress and strain can be assumed. The dominant variations in rheology of fecal matter are

in the viscosity which changes with local water content and potentially with the existence of a yield stress. Both regimes can be dealt with by suitable variations in the viscosity. From Cleary [22], a suitable form of the momentum equation for a Newtonian fluid with strongly variable viscosity is:

$$\frac{d\mathbf{v}_a}{dt} = \mathbf{g} - \sum_b m_b \left[ \left( \frac{P_b}{\rho_b^2} + \frac{P_a}{\rho_a^2} \right) - \frac{\xi}{\rho_a \rho_b} \frac{4\mu_a \mu_b}{(\mu_a + \mu_b)} \frac{\mathbf{v}_{ab} \mathbf{r}_{ab}}{\mathbf{r}_{ab}^2 + \eta^2} \right] \nabla_a W_{ab} \qquad (2)$$

where $P_a$ and $\mu_a$ are pressure and fluid viscosity of particle *a*. The velocity difference between particles is $\mathbf{v}_{ab} = \mathbf{v}_a - \mathbf{v}_b$ and $\mathbf{g}$ is the gravity vector. Here $\eta$ is a small parameter used to smooth out the singularity at $\mathbf{r}_{ab}=0$ and $\xi$ is a factor associated with the viscous term. Eq. (2) was formulated to give good momentum conservation in the presence of very high spatial viscosity gradients and has been successfully used for simulating solidification of metals during casting where the viscosity can vary by several orders of magnitude over short distances [23, 24]. Even though the computational method allows viscosity variation, we will make the additional assumption that the viscosity is constant. This is done to simplify this initial analysis of what is a complex fluid-structure system and because the length of bowel modelled here is fairly short restricting the amount of variation that is possible. When the model is extended to the full bowel, viscosity variation resulting from water concentration variation can be modelled by solving for the coupled diffusion of water through the system (in the same way as dissolved gas flow was modelled using SPH in [25]) and using this to control local fecal viscosity.

A quasi-compressible approach is used for linking the pressure and density of each particle using an equation of state:

$$P = P_0 \left[ \left( \frac{\rho}{\rho_0} \right)^{\gamma} - 1 \right]. \qquad (3)$$

Here $P_0$ is a problem specific pressure scale and $\rho_0$ is a reference density. We use $\gamma$ = 7 corresponding to the behavior of incompressible liquids. The timestep is given by the Courant-Friedrich-Lewy stability limit [18]. We model the fluid flow near the incompressible limit.

The intestinal model proposed uses a cylindrical geometry with periodic boundary conditions at each end of the tube. The boundary wall is visco-elastic and generates tensile forces if stretched

beyond its natural length in any direction. The tube is filled with just enough fluid such that there are no void spaces and so that there are no tensile forces generated in the walls when at rest.

The colon geometry is discretized to form a regular array of SPH boundary particles on the surface of the tube. Each pair of adjacent nodes is connected by a linear spring that allows for elastic deformation of the lumen and a dashpot that generates viscous damping. This network permits the boundary to flex in response to internal forces such as intra-luminal pressures and contractions generated by passing peristaltic waves. Figure 1 shows an example of the deformation of the boundary due to the passage of a peristaltic wave. The muscular forces that cause contraction and relaxation of the boundary are modeled by shortening the natural lengths of elastic elements in an affected region. Similarly, the relaxation of the muscles in the region of DI can be modeled by allowing the natural lengths of the elastic elements to lengthen. This is a powerful and effective model for an active boundary arising from the tightening or relaxing of circular muscle in the intestinal wall. The key advantage of this model is that the instantaneous shape of the wall is a direct prediction from the fluid-structure interaction between intra-luminal content and muscular control of the boundary. This is in contrast with earlier models where the wall deformations needed to be specified as inputs to the model thereby introducing significant uncertainty about the predictive capability of such models [12-14].

Travelling peristaltic waves are generated in the intestinal wall and travel in the antegrade direction. The wave consists of contraction (ascending excitation) and relaxation (DI) components that modify the instantaneous wall tensions in each longitudinal slice, as described above, as they pass by. The shape of the waveform in the intestinal wall is not known. Here, we maintain smooth variation with distance for each peristaltic wave using a cosine function so that the maximum contraction and expansion occur at the centre of each affected region and decreases to zero at the edges. The magnitude of the contraction/expansion varies in time with the wave development described by a sine function over time with the period being the period of the peristaltic wave. This waveform controls the natural lengths of the elastic wall elements and thereby produces the required degree of contraction or relaxation. It can move along the colon leading to a travelling contractile wave with a preceding DI. The operation of the model for the peristaltic wave emulates the real behavior of the

colon with a wave of muscular contraction propagating along the colon. Propagating sequences in the colon can therefore be represented by series of these waves.

## 3 Simulation and Model Parameters

The geometry of the intestinal section is 5 cm in diameter and 30 cm long representing a part of the colon. The elastic stiffness for the wall was 10 N/m and the viscous damping coefficient was 1.9 N.s/m. The fecal content for the base case had a density of 1.0 g/cm$^3$ and dynamic viscosity of 1 Pa.s.

A simple series of regular waves with 12 s intervals between them is used for this initial study. Each wave commences at the same position near the start of the tube and travels in the antegrade direction at a speed of 1.7 cm/s. Each contraction/relaxation waveform develops over 5.5 s until the point of maximum amplitude is reached and then declines over the next 5.5 s allowing the intestinal wall to relax. For the base case, a non-lumen occluding amplitude of 1 cm was used for both the radial contraction and relaxation components corresponding to a peak lumen occlusion of 40%. Note that the expansion in the DI region does not automatically occur. The colon wall locally is able to accommodate a 40% expansion but the actual development of the expansion needs to be driven by fluid pressure within.

Data attained through *in vivo* high-resolution colonic manometry [26] suggest that colonic contractions occur over 2-4 cm. For the base case of the model, we have chosen a length of 4 cm as a starting point. As we have no data on the estimated length of the descending inhibition region we have also chosen a length of 4 cm giving a combined length of 8 cm.

Simulations were performed with this coupled SPH-deformable wall-peristaltic wave model to investigate the role of DI in transport. Since many of the basic input data relating to the nature of the motor patterns are not known accurately, we conduct a series of parametric studies to examine the sensitivity of fluid transport to these important characteristics of the intestinal system. The specific cases simulated are summarized in Table 1. Specifically, the degree of occlusion was varied from 20 to 80% to investigate the effect of low- and high-amplitude waves on the predicted intra-luminal pressures and flow-field, and the length of the contraction/relaxation region was varied between 2

cm and 8 cm. We also investigate the influence of varying the fecal viscosity from fluid-like (0.01 Pa.s) to semi-solid-like (10 Pa.s).

## 4 Development of a Single Peristaltic Wave

We first consider the development of a single peristaltic wave travelling from left to right in a simulation of the base case conditions. The influence of the deforming lumen on the intra-luminal content is apparent in Figure 2. This shows the development of a single wave of contraction at three times over a period lasting from 1 s before the point of peak contraction/relaxation and up to the point of peak contraction/relaxation. Isosurfaces of longitudinal speed (Fig. 2a) and pressure (Fig. 2b) demonstrate modification of the flow field with the onset of the wave. The wave propagates in the antegrade direction (to the right) and the partially occluded lumen pushes into the fluid content in front of the contraction producing a rise in intra-luminal pressure of 10 Pa.

The initial part of the contraction generates a low-speed forwards-moving “bubble” of fluid (Figure 2a(i)). Evidence of the previous wave remains as a region of low pressure with reduced lumen diameter in the posterior half of the colon section (Figure 2b(i)). For sufficiently high fluid viscosity, there can be significant delay in redistribution of intra-luminal material (and therefore pressures) after a contraction. So although the fluid used here is Newtonian, there is evidence of a memory effect where an earlier wave can influence luminal occlusion well after it has passed. This history dependence means that subsequent waves can interact and affect the fluid transport rates, supporting the hypothesis that sequential patterns of contractions can affect fecal matter transport [3, 6].

Expansion of the lumen develops in the relaxation region (Figure 2a(ii)) and fluid immediately downstream of the contraction increases in speed. The region of antegrade directed flow now extends to around a third of the length of the colon section and the peak antegrade speed increases to 1.2 cm/s. Some retrograde flow develops upstream from the contraction. To conserve momentum in this system, antegrade flow is balanced by lumen movement in the retrograde direction. Pressure on the lumen in the contraction region and intra-luminal pressures downstream of the contraction both increase (Figure 2b(ii)). The redistribution of intra-luminal pressure upstream in response to the propagating contraction radially expands the upstream lumen back to its initial resting position.

The non-uniform distribution of pressures in the intra-luminal content develops as a consequence of the passing wave and is evident even for a non-lumen occluding event. This suggests that significant pressure changes do occur for partial occluding events and should be able to be captured by manometric measurements.

Figure 2a(iii) shows the fully developed peristaltic wave form. The region of antegrade directed flow has increased in speed to match the wave speed but decreased in size so that it is now fully contained within a compact volume inside the expansion region. This reduction corresponds to the decrease in intra-luminal pressure immediately downstream of the dilation due to re-pressurization of the posterior half of the colon section (Figure 2b(iii)).

## 5 Role of Descending Inhibition

In order to understand the role of the DI in motility we compare the case from the previous section with one where the DI is suppressed (and therefore where there is no relaxation of the circular muscle in advance of the contraction). The pressure and flow field in a vertical plane that passes through the middle of the colon are shown in Figure 3 for the two cases when the wave form has fully developed. The shaded color represents the fluid pressure with dark blue being low pressure and red being high pressure. The arrows show the velocity field of the flow. The arrows are colored by longitudinal speed with blue arrows showing retrograde and red showing antegrade flow and the length of arrow indicating longitudinal speed.

The case including DI is shown in Figure 3a. A high pressure zone is created in the right half of the contraction due to the antegrade motion of the peristaltic wave. To alleviate this pressure, the fluid in this region wants to expand sideways. The addition of muscular relaxation downstream of the contraction therefore allows the walls to expand. The expansion increases the intra-luminal space available causing a significant reduction in fluid pressure in the relaxed region so that it has a much lower pressure than that experienced to the left of the contraction. This means that there is a high pressure gradient directed to the right of the contraction and a much smaller pressure gradient to the left. Strong asymmetry in the pressure gradients leads to significant asymmetries in the fluid velocities generated. This leads to much faster flow to the right involving a much larger volume of fluid compared to the much smaller amount of fluid that moves to the left at a much lower speed.

Therefore strong net transport in the antegrade direction results when DI is present and transport volume is dependent on its size. Fluid near the walls travels at the same speed as the walls due to the no-slip boundary condition so there is continuity of the velocity field in the wall and adjacent fluid. To the right of the advancing contracting wall, fluid is directed radially inwards driving a central cylindrical jet of higher speed antegrade flow inside the DI. As the wall relaxes, the flow then diverges radially outwards into the expanded intra-luminal space. This drives a three-dimensional ring vortex that appears in the sectioned flow field in Figure 3a as a pair of recirculation vortices. This vortex influences the wall shape by controlling the pressure distribution along the walls in the DI, but the resulting wall shape also influences the size and shape of the vortex since they are two-way coupled. This recirculation zone will be important for transport and mixing. The identification of this flow structure is not new and fluid trapping (and the trapping of solid particles) inside similar recirculation zones has been observed in other peristaltic flow models that use prescribed wall shape and motions [27]. Inside the region where the walls are contracted we also see a strong jet of retrograde flow which extends just outside the region of the muscular contraction.

Figure 3b shows the case with muscular contraction only (without the DI). The length of this contraction was specified as 8 cm which is the same as the length of the combined contraction/expansion in the DI case. When the wave propagates without DI, the deformation of the lumen is symmetric in the longitudinal direction. The region of high pressure to the right of the contraction is similar to the case with the DI. The fluid pressures upstream and downstream of the contraction are low and of similar magnitude leading to strong flow in both directions from the region of high pressure. As for the case with DI, we observe a central jet of high speed antegrade flow in advance of the contraction. There is still weak evidence of a ring vortex but this is much smaller and less intense than that observed for the case with DI. Higher speed retrograde flow is visible inside the contraction region and extends further upstream outside the contraction. The walls upstream from the contraction very quickly relax back to their rest state. Due to the comparable antegrade and retrograde flow there is little net forwards transport (to the right) for the case without DI. High wall tension is observed with pressures in excess of 55 Pa along the length of the contraction.

This indicates that the addition of the DI provides a more efficient mechanism for fluid transport.in non-lumen occluding events. The reduction in wall tension when a DI is present also suggests that the colon walls may do less work in propagation of fecal content than if no relaxation were present.

## 6 Sensitivity of transport to the fecal properties and peristaltic wave form

### 6.1 Effect of Viscosity of Colonic Content

Dewatering of fecal matter during its passage along the colon can produce viscosity variations of orders of magnitude along the length of the colon from fluid-dominated at the start of the colon to semi-solid at the rectum. To better understand the effect of viscosity on the flow and pressure field for a single contraction, we predict coupled flow and bowel wall behavior for the fecal viscosities of 0.01, 0.1, 1 (the base case), 3.0 and 10 Pa.s. All other conditions are kept the same as for the base case. Figure 4 shows the flow inside the colon and the corresponding pressure distribution for the five intra-luminal viscosities. The coloring scheme and the arrows are the same as for Figure 3.

Firstly, we consider the changes in flow and pressures in the colon as we reduce viscosity with respect to the base case (Figure 4c). For 0.1 Pa.s (Figure 4b) the length of the contracted region at the left end of the peristaltic wave is now shorter in the upstream longitudinal direction. There is a reduction in pressure just upstream from the contraction that leads to an increase in volume of retrograde flow with increased peak velocities and more rapid relaxation of the upstream walls back to their rest position. In addition, pressures immediately in front of the contraction decrease resulting in less expansion of the walls in the relaxation region and lower peak pressures along the walls in this region. In the DI, the ring vortex is modestly smaller but more intense due to the reduced intra-luminal space in that region. Peak antegrade flow velocities increase mildly inside the DI and downstream from the DI there is low-speed antegrade flow in advance of the travelling wave.

Reducing the viscosity further to 0.01 Pa.s (Figure 4a), causes the contracted region to become more compact in the longitudinal direction. Upstream pressures reduce further leading to an increase in peak retrograde flow velocities such that the walls immediately upstream of the contraction have fully relaxed back to their rest position. The mobilized volume now extends a small distance out from the contraction region and along the walls there is a narrow region of high

retrograde flow. Due to the no-slip condition at the boundary, this implies that the walls themselves are moving to the left which is a consequence of conservation of momentum in this untethered system. The pressures to the right of the contraction (antegrade) are also much reduced and there is further reduction of the higher pressures observed along the wall in the relaxation region. The reduced pressures in front of the contraction lead to further reduced expansion of the walls in the relaxation region and the recirculatory flow in the ring vortex becomes less intense. There is a further increase in the volume of antegrade flow which now extends from the right of the relaxation region to well across the periodic boundary.

Next we consider the impact of increasing viscosity. For 3 Pa.s (Figure 4d), the peak wall contraction is mildly reduced, but the axial length of the contracted region is comparable to the base case. Pressures are much higher from the point of peak contraction up to around one-third of the way into the DI. Pressures in the downstream half of the DI are reduced which results in less wall expansion in this region and the development of mild longitudinal asymmetry in the shape of the DI. Adjacent to the walls, pressures become much higher extending along the wall from the peak contraction to the peak relaxation. The reduced wall contraction is due to the much higher pressures at the wall which oppose the force of the muscular contraction. At the start of the DI, there is very strong flow that is forced radially inwards by the advancing contraction. Flow circulation in the DI (previously observed as a vortex ring) is now modified so that the flow no longer forms a fully closed loop and is instead directed further downstream of the point of peak relaxation. This flow structure shrinks slightly and is shifted left towards the contraction. Antegrade flow decreases in velocity and becomes confined to inside the DI. Retrograde flow velocities also decline and flow now commences from the upstream side of the contraction but extends as weak retrograde flow upstream.

Increasing viscosity further to 10 Pa.s (Figure 4e) the contracted length of the wall now extends a much greater distance to the left of the applied muscular contraction. At higher fluid viscosities, increased resistance to flow means that the content is less mobile and pressures take longer to redistribute. Thus the upstream walls take longer to relax back to their rest state and therefore the length of the observed contracted region is much longer than the length of the muscular contraction.

The degree of maximum wall contraction in the contracted region is now much smaller. The reduced mobility of fluid at this viscosity leads to a build-up of pressure immediately to the right of the peak wall contraction which extends all the way through this region and halfway into the relaxation region. There are higher pressures observed adjacent to the contracted wall which oppose the force of the muscular contraction resulting in a smaller degree of contraction. The wall expansion in the relaxation region is also greatly reduced. This is due to large-scale changes in the pressure distribution for this viscosity. The radial pressure gradient across the tube is now much lower in this region and there is an increase in longitudinal pressure gradient. There is a strong decline in retrograde and antegrade flow velocities and the ring vortex is no longer discernable.

Figure 5 shows the rate of volumetric transport that is measured as a single peristaltic wave crosses a specific longitudinal position for four viscosities. Overlaid on the figure are vertical dashed lines representing the times when characteristic parts of the peristaltic wave cross this position. The leading edge of the DI relaxation (marked by line A) arrives first followed by peak of the DI (line B), the neutral center of the wave (line C), the peak contraction (line D) and the end of the contraction (line E).

The base case (1 Pa.s) shows some initial retrograde flow just prior to the arrival of the front of the DI (point A). This is due to the wake from a previous wave. There is a large positive flow peak of 34 $cm^3/s$ (between points B and C) which corresponds to strong antegrade transport by the DI. Note that the peak flow lags the peak of the physical expansion as the fluid takes some time to respond. The flow rate then steadily decreases and at the neutral point between the contraction and relaxation phases of the wave it has declined to 12 $cm^3/s$. Inside the contraction region, the flow reverses direction and we see a large negative flow peak of 15 $cm^3/s$. Whereas the peak antegrade flow lags behind the peak DI, the peak retrograde flow lags behind the peak physical contraction. The negative flow rate then steadily decreases but over a much longer period than the antegrade flow. Therefore, the net transport rate for this system is 4.7 $cm^3$/wave.

Reducing the viscosity to 0.1 Pa.s, there is a mild reduction in the positive flow peak and the peak occurs earlier so the lag of the antegrade flow behind the peak DI is much smaller. Transport drops to nearly zero at point C. The increased fluid mobility is responsible for a 50% increase in

retrograde transport past the partial-occluding contraction. Following the contraction, retrograde transport decreases at a much greater rate than for the base case. Once the wave has passed the flow again reverses direction and there is a short duration pulse of antegrade flow as the system relaxes back to its resting state. These effects give an increased net transport rate of 7.4 $cm^3$/wave.

For 0.01 Pa.s, there is a 15% decrease in the positive flow peak from the previous case. The peak also occurs mildly earlier so that there is no lag behind the peak DI for this viscosity. The negative peak is comparable in magnitude to the previous case. Again there is a small secondary positive flow peak following after the wave has passed whose peak is mildly higher for the 0.01 Pa.s case. The net transport rate for this case is further increased to 15.6 $cm^3$/wave. So there is a substantial improvement in transport efficiency for viscosities below 1 Pa.s.

Next we consider viscosities higher than the base case. For 3 Pa.s, the peak antegrade flow rate decreases by 30% and is much delayed behind the peak DI, occurring two-thirds of the way between B and C. The flow rate falls to zero halfway between points C and D. There is a reduction of 30% in the peak retrograde flow and a small additional lag behind the peak contraction now occurring halfway between points D and E. Just after the trailing edge of the wave (point E), there is further weak retrograde transport very similar to that of the base case. There is no evidence of the secondary positive flow peak observed at lower viscosities. The net transport rate for 3 Pa.s is reduced to 3.8 $cm^3$/wave.

Increasing to a viscosity of 10 Pa.s, the peak antegrade flow rate decreases by 70% from the 3 Pa.s case and there is an almost constant peak rate from B to C. Antegrade transport occurs over a longer period of time from point A almost up to point D (the peak contraction). The flow rate falls to zero at a similar time to the 3 Pa.s case. Much weaker retrograde transport (with a peak flow rate reduced by 65%) then occurs from this point until well after the trailing edge of the wave. So, at higher viscosities the DI is observed to contribute less to transport. The transport behavior therefore changes from one where low pressures in the DI create positive thrust to one where the contraction forces fluid forward albeit less efficiently so that there is a reduction in net transport rate to 3.4 $cm^3$/wave.

Figure 6 shows the variation of the net transport rate for the different viscosity cases. The dashed curve is a fit to the data points using regression. The functional form of the relationship between transport rate and fluid viscosity is an inverse power law with an exponent of 0.25. The goodness of this fit is 0.99. In partial occluding contractions, transport becomes considerably more effective for low viscosity content with a five-fold increase occurring for the three orders of magnitude viscosity variation considered here. This is primarily due to the increasing importance of the DI at low viscosities in producing thrust.

Figure 7 shows the pressure recorded by a number of virtual pressure sensors placed at different radial distances (1, 1.5 and 2 cm) from the colon longitudinal axis for viscosities of 1 and 10 Pa.s. Overlaid on the figure are vertical dashed lines representing the times when characteristic parts of the peristaltic wave cross this position as per Figure 5. The longitudinal position of these sensors corresponds to the same measurement location as for the transport rates above, so we can directly relate the results from Figure 5 and 7. These sensors are intended to mimic the operation of real manometric sensors in-vivo, and give pressure traces that can be compared with real measurements. Figure 7a shows the sensor measurements for a viscosity of 1 Pa.s. The pressures at each sensor steadily rise while there is positive antegrade transport (inside the DI region) and the two inner radial sensors reach a common peak pressure of 10 Pa at the point where the neutral part of the wave crosses the sensors (point C). From point C to E, the sensors at 1 and 1.5 cm show steadily declining pressures until the trailing end of the contraction passes them. They both show some oscillatory structure in the pressures at low viscosities. In contrast, the pressure at the outer radial sensor continues to rise sharply in the contraction region to a peak of 38 Pa at the point of maximum contraction (point D). This occurs because the sensor is close to the contracting walls and the high pressure is generated to force the fluid to move in front of the contracting wall surface. So there is a high local pressure gradient in the outer radial half of the colon. The pressure gradient is close to zero in the inner half of the colon. The peak pressure then rapidly declines and overshoots with a small negative peak of 5 Pa corresponding to suction near the walls as the contraction wanes and the walls move back towards their neutral position. The pressures recorded by such sensors are therefore dependent on their radial position.

Figure 7b shows sensor measurements for viscosity 10 Pa.s. The pressure behavior is quite different. There is an initial decline in pressure as the (now much smaller) DI region crosses the sensor locations with the peak suction pressure increasing with radius. In all three locations the pressure then increases rapidly to a peak pressure that occurs inside the contraction region followed by a decline back to equilibrium pressure. For the inner radial sensors, the peak occurs close to point C, but for the outer radial sensor it is delayed until a point one third of the way between C and D. The peak pressures at 1 and 1.5 cm are again little different to each other but higher at around 14 Pa than was the case for the lower viscosity. The peak pressure at 2 cm is now only 17 Pa which is only mildly higher than for the other radial positions, but less than half the peak value for the lower viscosity. So there is only a mild radial pressure gradient and therefore little radial contribution to the motion of the fluid. As seen in Figure 4, there is a strong band of high pressure across the colon with little radial variation but with strong axial variation. The strong axial pressure gradient is what generates the motion of the fluid. There are also no stages with suction pressures as the walls retreat at the end of the contraction. So a key effect of viscosity change is to control the degree of localization of the fluid flow and to control the magnitude of the radial variation in pressure. For low viscosities, only fluid close to the moving walls is mobilized and this is done by large pressure gradients that have a strong radial component which then generates inward strong radial flow that in turn drives the ring vortex. For high viscosity, the influence of the walls is felt by fluid at all radial locations, there is little radial pressure variation and the resulting flow is almost entirely axial. It is therefore reasonable to expect that the pressures recorded by real manometric sensors are also likely to be a function of the intra-luminal viscosity.

The detailed structure of the flow and how propulsion is generated varies strongly with viscosity. Since stool viscosity can change considerably over the entire length of the large intestine, this means that there is considerable change in the fluid dynamics of the stool along its length. Transport is most effective at lower viscosities. At high viscosities (> 3 Pa.s), the transport behavior changes from low pressures in the DI contributing positive thrust to the contraction alone forcing fluid forwards. Consequently, the radial pressure gradient also depends on viscosity and measurements from manometric sensors will depend on their radial position. In addition, viscosity

controls the time taken for the system to relax back into its natural state following the passage of a peristaltic wave. The coupled wall-fluid system has memory on a viscous relaxation timescale. Therefore the time for the system to relax is longer for high viscosity content and this suggests that the interaction between sequential patterns of contractions and their combined effect on fecal transport may be viscosity dependent. The recirculation vortex ring is important for transport, mixing and pressure distribution in the DI and it depends strongly on viscosity. The vortex in the DI diminishes in size and strength at high viscosities which affects the flow directed radially outwards to the walls and therefore the wall expansion in the DI. This also suggests that mixing of fecal matter via this mechanism will tend to be stronger for lower viscosity content.

### 6.2 Effect of Degree of Contraction of Tube (lumen occlusion)

Next we investigate the effect of the degree of contraction on the flow field. For a single viscosity (the base case with viscosity 1 Pa.s), we vary the applied muscular force leading to different degrees of lumen occlusion. These are 20%, 40% (base case), 60% and 80% measured as the % of occlusion of the cross-sectional area of the tube.

Figure 8 shows the flow inside the colon and the corresponding pressure distribution for the 40% (base) and 80% occluded cases. The coloring scheme and the arrows are the same as for Figure 3. The increased strength of the muscular contraction and relaxation for the 80% occlusion causes changes in wall shape, fluid pressures and flow field. The length of contracted region in the wake of the muscular contraction is much longer than for the base case indicating that it takes much longer for the system to relax back to a resting state following the passing of a high amplitude contraction. In the region of DI, there is a 30% increase in maximum wall expansion. This is in response to the higher pressures in the fluid immediately in front of the contraction which extend from the contraction up to the point of peak relaxation. Higher pressures are observed along the walls (especially around the point of peak contraction) and extend throughout the relaxation region. There is an increase in peak antegrade velocities in the DI. The recirculation vortex grows in size (with the increase in intra-luminal space) and strength, and its centre shifts slightly left towards the contraction. Where the edge of the vortex meets the leading edge of the contraction, there is strong radially inward flow observed. The average retrograde flow velocities are not significantly different to

the base case but for the 80% occlusion retrograde flow now occurs throughout the full length of the much longer contracted region. Therefore the volume of mobilized fluid travelling in this direction increases resulting in a small increase in retrograde transport.

Figure 9a shows the rate of volumetric flow crossing a specific longitudinal position for the four occlusion levels. As in Figure 5, we overlay vertical dashed lines representing the times when parts of the peristaltic wave cross this position. Firstly, we consider the effect of reducing the degree of occlusion from 40% to 20% so that the lumen now penetrates a smaller distance into the flow. At 20% occlusion, the relaxation time for the system is short enough that the walls relax back to their natural state before the arrival of the next wave. Therefore the transport rate is approximately zero before the leading edge of the next wave arrives. There is a reduction of the positive flow peak by 45% and a reduction in the retrograde flow peak by 40%. These occur at the same times as for the 40% occluded case. The net transport declines to just 1.3 $cm^3$/wave.

For the 60% occlusion, there is increased retrograde flow prior to the arrival of the leading edge of the wave. The peak antegrade flow increases by 35% and occurs at the same time as the peak for the base case. The peak retrograde flow increases by 25% but lags further behind the peak contraction occurring two-thirds of the way between D and E. The net transport rate increases to 9.1 $cm^3$/wave.

For an 80% occlusion, there is greater retrograde flow prior to point A. Just before point B, a new higher flow peak of 78 $cm^3$/s, occurs that is not observed for the other occlusion cases. The second antegrade flow peak increases by an additional 30% compared to the 60% occlusion case with the peak still occurring at the same time as the previous cases. The peak retrograde flow increases by an additional 20% and lags further behind the peak contraction occurring just after the trailing edge of the wave has passed (point E). The net transport rate increases further to 25.2 $cm^3$/wave. Transport is observed to be much more efficient for high amplitude waves.

Transport depends strongly on the degree of occlusion. With greater occlusion, the peak antegrade flow rate increases (and the peak retrograde flow rate increases although less strongly) giving an overall rise in the net volume of fluid transported. The period of antegrade flow and the point at

which the peak forwards transport lags behind the peak DI do not change with the degree of occlusion.

Figure 9b compares the transport rate for two partial occlusion cases (40% and 80%) at a higher viscosity of 10 Pa.s. The increase in occlusion causes the peak antegrade flow rate to increase by 160%. There is also an increase in the lag time that this peak trails behind the peak muscular relaxation which now occurs just before point C. In addition, antegrade flow occurs over a slightly longer period. The peak retrograde flow increases by 85% and coincides with the trailing edge of the wave at point E. These effects (increased occlusion and viscosity) together increase the net transport rate in the antegrade direction by approximately five-fold. So there are significant gains in the transport of high viscosity content when using high amplitude contractions even though the degree of retrograde transport is also moderately increased. Broadly, the behavior at high viscosity with increasing degree of occlusion follows the same trends observed at low viscosities (as discussed for Figure 9a) with one exception. The lag of the peak antegrade transport behind the peak relaxation depends not only on the viscosity (as observed in the previous section) but also on the degree of occlusion as well. Therefore at very high occlusion and high viscosity the peak transport occurs immediately in advance of the neutral part of the wave.

Figure 10 shows the variation of the net transport rate with occlusion amplitude for viscosities of 1 Pa.s and 10 Pa.s. An exponential function is fitted to the 1 Pa.s data using regression and is shown as the dashed curve. The fitted exponential coefficient is 4.78 and the goodness of fit is 0.99. Therefore there is an exponential increase in transport with increasing degree of occlusion for the 1 Pa.s case such that transport increases twenty-fold for a four-fold reduction in open area of the contraction. At higher viscosity (10 Pa.s) transport also increases with degree of occlusion so that there is a five-fold increase in transport when the open area of the contraction is halved. This indicates that for a given viscosity the transport rate in the colon is controlled by the amplitude of contraction and that transport is significantly more effective at high occlusion.

In normal colonic function a range of different wave amplitudes is typically measured along the full length of the large intestine, but the roles that low and high amplitude waves play in mixing and transport are not yet understood. Transport rate improves for contractions that lead to greater lumen

occlusion. In particular, high occlusion appears to be especially important for transporting high viscosity content. The length of the upstream contracted region trailing the wave is much larger for larger contractions. This suggests that the timescale for memory stored in the system will also depend on the degree of contraction of the lumen. So for contractions that lead to high occlusion there is an increase in the relaxation time for the system. This means that sequences of high amplitude contractions will tend to experience greater overlap between successive contractions than occurs for low amplitude contractions and so this may influence transport for sequential patterns of contractions.

### 6.3 Length of Peristaltic Wave

The length of the real contractions is not known and state-of-the-art manometric sensor data is limited to coarse spatial sampling (~ 1 cm steps) along the full colonic length [26]. Understanding how the pressure field is influenced by the size of the contraction will help differentiate between single coherent propagation waves and possible multiple short-length waves moving in different directions. Here, we consider the effect of the length of the entire contraction/relaxation region on the flow and transport. Figure 11 shows the flow inside the colon and the corresponding pressure distribution for three different lengths of peristaltic wave (2 cm, 4 cm and the base case of 8 cm). Considering the 4 cm wave (Figure 11b) in relation to the base case (Figure 11a) we observe that the degree of occlusion for the 4 cm wave is comparable to that of the 8 cm wave for the same applied contractile force, but there is significantly less expansion of the walls in the relaxation region. This leads to a rise in pressures within the central space of the DI which significantly reduces peak antegrade flow velocities, although there is small antegrade flow observed right up until the periodic boundary. The vortex length significantly decreases in size and intensity and shifts back towards the contraction. Increased pressures at the wall are observed from the right of the relaxation region all the way to the edge of the periodic boundary. The peak retrograde flow velocities are comparable to the base case, but these now extend a shorter distance out from the contraction. The 2 cm wave case (in Figure 11c) shows less occlusion by the contracting wall and very little dilation of the walls in the DI. Pressures inside the contraction region are smaller and this has a marked effect in reducing both antegrade and retrograde flow velocities. The vortex is no

longer visible. A mild pressure gradient can be seen in the longitudinal direction that extends to the right of the DI and all the way to the downstream end of our colon segment. This drives small bulk antegrade flow along this entire region. Compared to the 4 cm wave, peak pressures at the wall become highly localized to the right of the contraction. In addition there is a reduction of pressures along the wall from the DI and to the right up until the periodic boundary. There is a mild reduction in peak retrograde velocities and retrograde flow extends a shorter distance to the left out of the contraction region.

Figure 12 shows the rate of volumetric flow measured crossing a single longitudinal position for the three wave lengths. Again, as in Figure 5 we overlay vertical dashed lines representing the times when characteristic parts of the peristaltic wave cross this position. The base case initially showed some retrograde flow prior to the arrival of the DI part of the wave. However as we had already seen in Figure 11 there is bulk antegrade flow that precedes the travelling wave for both the 2 cm and 4 cm waves. This is evident in the positive flow rates observed in advance of point A (the leading edge of the DI) for both cases. For the 4 cm wave relative to the base case, there is a 30% decrease in peak antegrade flow and the arrival of this peak lags behind the base case occurring at a time halfway between points B and C. The peak retrograde flow is reduced by 15% and occurs prior to point D, whereas the peak for the base case occurs after point D. The reduction in retrograde flow then falls off more rapidly in the wake of the contraction than for the base case. These modifications to the antegrade and retrograde flow result in a net transport rate that is reduced by 30%.

For a 2 cm length of wave, we observe an almost steady but mild increase in flow rate with time starting about 2 s before point A and reaching a peak just before point C (the neutral part of the wave). This rate of antegrade flow is much less than the peak rate for the other two cases and also less than the peak retrograde flow rate. However, the weak antegrade flow occurs over a much longer period than the retrograde flow such that the combined net flow is reduced to 2.4 $cm^3$/wave. Therefore we see a marked decline in net volumetric transport when decreasing the length of the peristaltic wave from 8 cm down to 2 cm. From Figure 11, there is substantial variation in the pressure field for such short length waves so we can expect them to be detectable in high-

resolution manometry data. However they will contribute less to transport than waves of greater length. In addition, they do not appear to play a role in the mixing of content due to the loss of the recirculation zone at these lengths.

## 7 Conclusions

This study introduces a new computational model for the coupled wall flexure and flow dynamics inside the colon subject to peristaltic waves of contraction and relaxation. The SPH method was used to describe the flow of intra-luminal content and the wall deformation was modeled as an active boundary using a visco-elastic spring network where the radial contraction and relaxation of circular muscle arise from changes in muscle tension inside the intestinal walls. Travelling waves were generated inside the intestinal walls with contraction and relaxation components.

The Descending Inhibition (DI) was shown to be an important physical mechanism for peristalsis in the colon. It appears to enable efficient transport for a compact region of content as well as reduced muscular work, even for partial occlusion of the lumen. This is due to the reduction in luminal and intra-luminal pressures inside the region of DI which generates positive thrust for the fluid volume contained inside the dilated region. A recirculation vortex forms inside the DI and is important for transport, mixing and pressure distribution in the colon. Factors which suppress DI (and therefore the development of this vortex) may lead to impaired motility and poor mixing and therefore may be linked to some aspects of colonic disease. Also, the system is able to demonstrate history dependence due to long delays in redistributing viscous intra-luminal material and pressure along the colon after the passage of a contraction. This means that there can be interaction between consecutive overlapping contractions whose pattern and timing can influence fecal transport.

Fecal viscosity controls both the degree of localization of the fluid flow and the magnitude of the radial variation in pressure. This has implications for interpreting measurements from manometric sensors inside the colon since the pressures recorded will depend on both viscosity and the radial position of the sensor. Dewatering of fecal content along the colon means that different regions of the colon can experience very different fluid dynamics of the stool based on the local viscosity. Transport improves with decreasing viscosity for a given degree of occlusion due to the increasing importance of DI. At low viscosities, a high radial pressure gradient drives the recirculation vortex in

the DI region. At high viscosities the transport behavior changes to one where the contraction forces fluid forward with little radial pressure variation leading to a weaker recirculation vortex and the flow becoming almost entirely axial with less wall expansion.

The degree of occlusion of the lumen was also found to strongly affect the transport rate. High occlusion contractions produce much greater forwards transport and are particularly effective for high viscosities. This suggests that coordinated neuromuscular activity in the walls is capable of localized control of transport rates in the colon by varying the amplitude of muscular contraction. The timescale for memory of the coupled fluid-wall system depends on both viscosity and degree of occlusion. So high amplitude contractions for highly viscous material may increase the extent to which the effect of successive waves can overlap and influence transport. Decreasing length of the peristaltic wave leads to decreasing transport rates as the recirculation zone vanishes for waves that are much shorter than the lumen diameter. This suggests that such waves will play at best a small role in the mixing of content.

This study has highlighted a number of factors that are important for understanding how the fluid dynamics in a partially occluded section of colon controls transport. This work is an important first step in establishing a framework within which clinicians may improve their interpretation of patient manometric data and how it pertains to motility. Extensions of this model will include the addition of the longitudinal contractions of the taenia coli (and the formation of haustral pouches), the natural convolution of the human colon, variation of colon diameter with length, the addition of regions of increased muscular tone and multiphase variation of fecal content.

**Acknowledgements**

Dr Sinnott, Dr Cleary and Dr Arkwright are all supported by funding from CSIRO, Australia. Dr Dinning is supported by NHMRC grant #630502 and the Clinician's Special Purpose Fund of the Flinders Medical Centre, Australia. Many thanks to Miss Cyndi Wang through the CSIRO Graduate Fellow program for assistance in prototyping the flow simulations and preliminary visualization.

**References**


1. N.A. Koloski, N.J. Talley and P.M. Boyce, Epidemiology and health care seeking in the functional GI disorders: a population-based study, Am J Gastroenterol 97, 2290-2299 (2002).

2. J.E. Pandolfino S.K. Ghosh, J. Rice, J.O. Clarke, M.A. Kwiatek and P.J. Kahrilas, Classifying esophageal motility by pressure topography characteristics: a study of 400 patients and 75 controls, Am Journal Gastroenterol 103, 27-37 (2008).

3. P.G. Dinning, M.M. Szczesniak and I.J. Cook, Proximal colonic propagating pressure waves sequences and their relationship with movements of content in the proximal human colon, Neurogastroenterol Motil 20, 512-520 (2008).

4. A. Ouyang, and G.R. Locke 3rd, Overview of neurogastroenterology-gastrointestinal motility and functional GI disorders: classification, prevalence, and epidemiology, Gastroenterol Clin North Am 36, 485-98 (2007).

5. S.S. Rao, P. Sadeghi, J. Beaty and R. Kavlock, Ambulatory 24-hour colonic manometry in slow-transit constipation, Am J Gastroenterol 99, 2405-2416 (2004).

6. P.G. Dinning, N. Zarate, L.M. Hunt, S.E. Fuentealba, S.D. Mohammad, M.M. Szczesniak, D.Z. Lubowski, S.L. Preston, P.D. Fairclough, P.J. Lunniss, S.M. Scott and I.J. Cook, Pancolonic spatiotemporal mapping reveals regional deficiencies in, and disorganization of colonic propagating pressure waves in severe constipation, Neurgastroenterol Motil 22, e340–e9 (2010).

7. Misra, J.C. and Pandey, S.K., Peristaltic transport of physiological fluids, Biomathematics: modeling and simulation, ed. Misra, J.C., pp 177-189, World Scientific (2006).

8. Grotberg, J.B. and Jensen, O.E., Biofluid mechanics in flexible tubes, Annu. Rev. Fluid Mech., 36, 121-147 (2004).

9. E.O. Carew and T.J. Pedley, An active membrane model for peristaltic pumping: Part 1. Periodic activation waves in an infinite tube, ASME J. Biomech. Eng 119, 66-76 (1997).

10. J.G. Brasseur, M.A. Nicosia, A. Pal and L.S. Miller, Function of longitudinal vs circular muscle fibers in esophageal peristalsis, deduced with mathematical modeling, World J Gastroenterol 13, 1335-46 (2007).

11. M.A. Nicosia and J.G. Brasseur, A mathematical model for estimating muscle tension in vivo during esophageal bolus transport, J Theor Biol 219, 235-55 (2002).

12. H.S. Udaykumar, S. Krishnan, S. Dillard, J.S. Marshall and K. Schulze, Computation of peristaltic transport and mixing in the small intestine, J. Biomech. 39 (Suppl); S422 (Abstract) (2006).

13. A. Pal, K. Indireshkumar, W. Schwizer, B. Abrahamsson, M. Fried and J. Brasseur, Gastric flow and mixing studied using computer simulation, Proc. R. Soc. Lond. B 271, 2587-2594 (2004).

14. M.J. Ferrua and R.P. Singh, Modeling the fluid dynamics in a human stomach to gain insight of food digestion, J. Food Sci. 75, R151-R162 (2010).

15. V.M. Bayliss and E.H. Starling, The movements and innervations of the small intestine, J. Physiol. 24, 99-143 (1899).

16. I.J. Cook, S.J. Brookes and P.G. Dinning, Sensory and Motor Function of the Colon. In: M. Feldman, L.S. Friedman and L.J. Brandt, editors. Gastrointestinal and Liver Disease 9th Edition. Philadelphia: Sleisenger and Fordtran's, p. 1660-1674 (2010).

17. S.K. Sarna, Enteric descending and afferent neural signaling stimulated by giant migrating contractions: essential contributing factors to visceral pain, Am J Physiol Gastrointest Liver Physiol 292, G572-581 (2007).

18. J.J. Monaghan, Smoothed Particle Hydrodynamics, Rep. Prog. Phys 68, 1703-1759 (2005).

19. P.W. Cleary, M. Prakash, J. Ha, N. Stokes and C. Scott, Smooth particle hydrodynamics: status and future potential, Progress in CFD 7, 70-90 (2007).

20. M.D. Sinnott and P.W. Cleary, An investigation of pulsatile blood flow in a bifurcation artery using a grid-free method, Proceedings. 5th Int Conf on CFD in Process Industries, Melbourne (2006).

21. M. Sinnott and P.W. Cleary (2009), Effect of rotor blade angle and clearance on blood flow through a non-pulsatile, axial, heart pump, Progress in CFD 10, 300-306 (2010).

22. P.W. Cleary, Modelling confined multi-material heat and mass flows using SPH, App Math Model 22, 981-993 (1998).

23. P.W. Cleary, J. Ha, M. Prakash and T. Nguyen, 3D SPH Flow Predictions and Validation for High Pressure Die Casting of Automotive Components, App. Math. Modelling 30, 1406-1427 (2006).

24. P.W. Cleary, Extension of SPH to Predict Feeding, Freezing and Defect Creation in Low Pressure Die Casting, App. Math. Modelling 34, 3189--3201 (2010).

25. P.W. Cleary, S.H. Pyo, M. Prakash and B. K. Koo, Bubbling and Frothing Liquids. ACM Transaction on Graphics, 26-3, Article No. 97 (2007).

26. J.W. Arkwright, I.D. Underhill, S.A. Maunder, N. Blenman, M.M. Szczesniak, L. Wiklendt, I.J. Cook, D.Z. Lubowski and P.G. Dinning, Design of a high-sensor count fibre optic manometry catheter for in-vivo colonic diagnostics, Optics Express 17, 22423-22431 (2009).

27. K. Connington, Q. Kang, H. Viswanathan, A. Abdel-Fattah and S. Chen, Peristaltic particle transport using the lattice Boltzmann method, Physics of Fluids 21, 053301 (2009).

| | *DI?* | $\mu$ (Pa.s) | % occlusion | Length of wave (cm) | Net Volume Transported ($cm^3$/wave) |
|---|---|---|---|---|---|
| Base case | *yes* | 1 | 40 | 8 | 4.7 |
| No DI | *no* | 1 | 40 | 8 | 2.5 |
| Viscosity 0.01 | *yes* | 0.01 | 40 | 8 | 15.6 |
| Viscosity 0.1 | *yes* | 0.1 | 40 | 8 | 7.4 |
| Viscosity 3.0 | *yes* | 3 | 40 | 8 | 3.8 |
| Viscosity 10.0 | *yes* | 10 | 40 | 8 | 2.6 |
| 20% Occluded | *yes* | 1 | 20 | 8 | 1.3 |
| 60% Occluded | *yes* | 1 | 60 | 8 | 9.1 |
| 80% Occluded | *yes* | 1 | 80 | 8 | 25.2 |
| High Viscosity; High Occlusion | *yes* | 10 | 80 | 8 | 16.1 |
| 2 cm long wave | *yes* | 1 | 40 | 2 | 2.4 |
| 4 cm long wave | *yes* | 1 | 40 | 4 | 3.4 |

Table 1: Summary of SPH colonic flow simulations performed and grouped into the individual parametric studies for role of DI; fecal viscosity; degree of occlusion; and length of peristaltic wave. The average volume of fluid transported antegrade in one 12 second period from the start of one wave to the next is shown in the right hand column for each case.

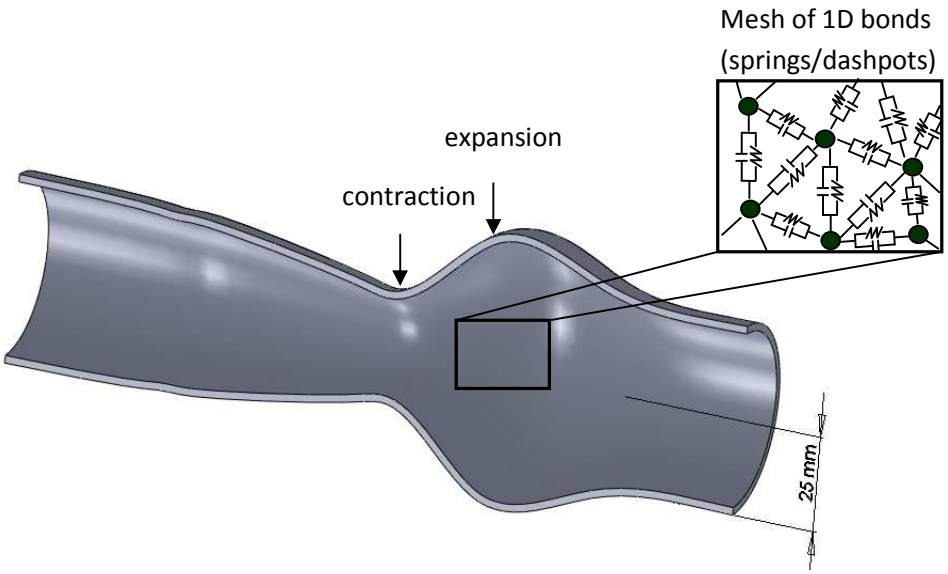


Figure 1: Picture of the deformation of the intestinal wall model used in this study. Part of the spring/dashpot network is shown inset.

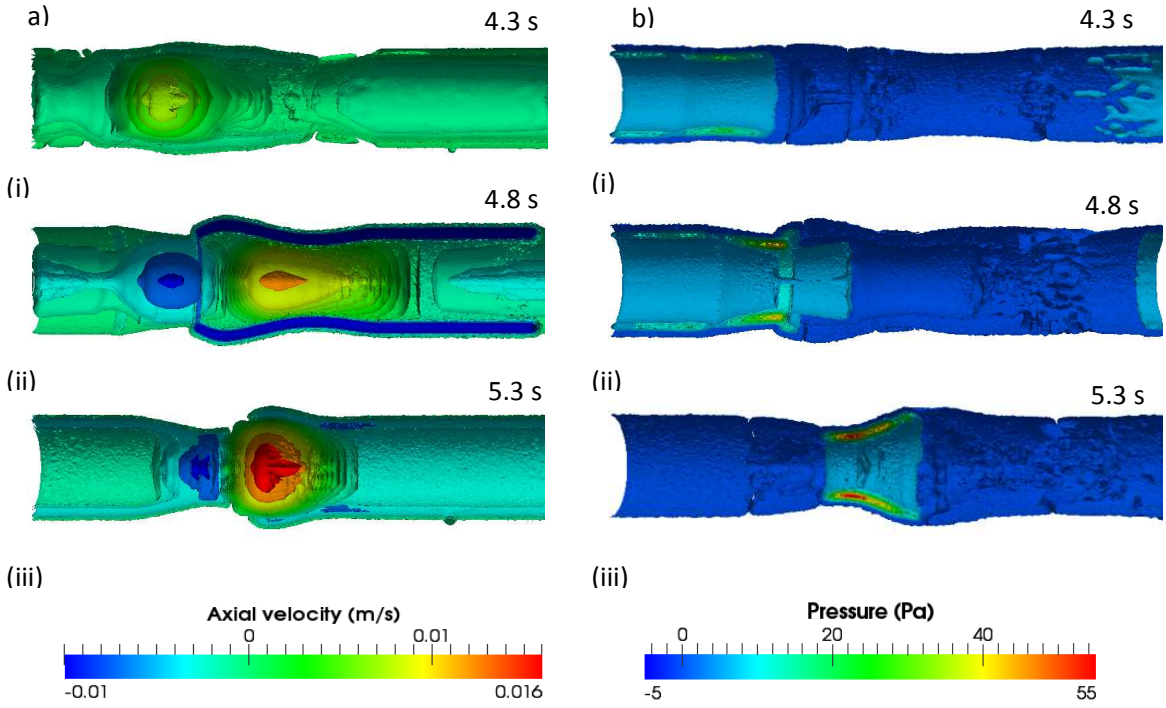


Figure 2: The development of the peristaltic wave for the case with DI shown at three different times (i, ii, iii) in the 11 second wave period. a) Isosurfaces of longitudinal velocity demonstrate antegrade (red) and retrograde (blue) flow. b) Isosurfaces of pressure show the non-uniform distribution of pressure in the intra-luminal content.

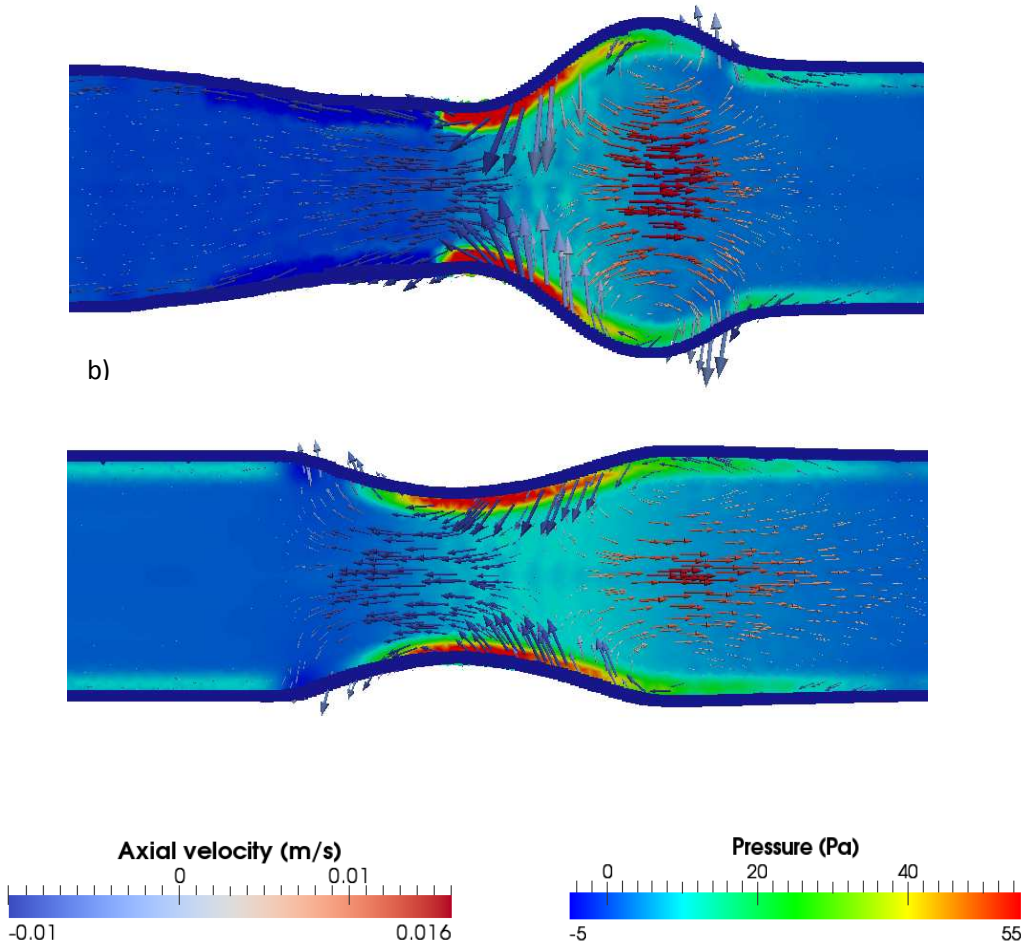


Figure 3: Vertical slice through the centre of the lumen with intra-luminal content (fluid) color-shaded from blue to red by pressure for the cases: a) contraction with DI included; and b) without DI. Velocity arrows are colored by longitudinal speed for antegrade (red) and retrograde (blue) flow and the arrow length represents longitudinal speed.

a) 0.01 Pa.s

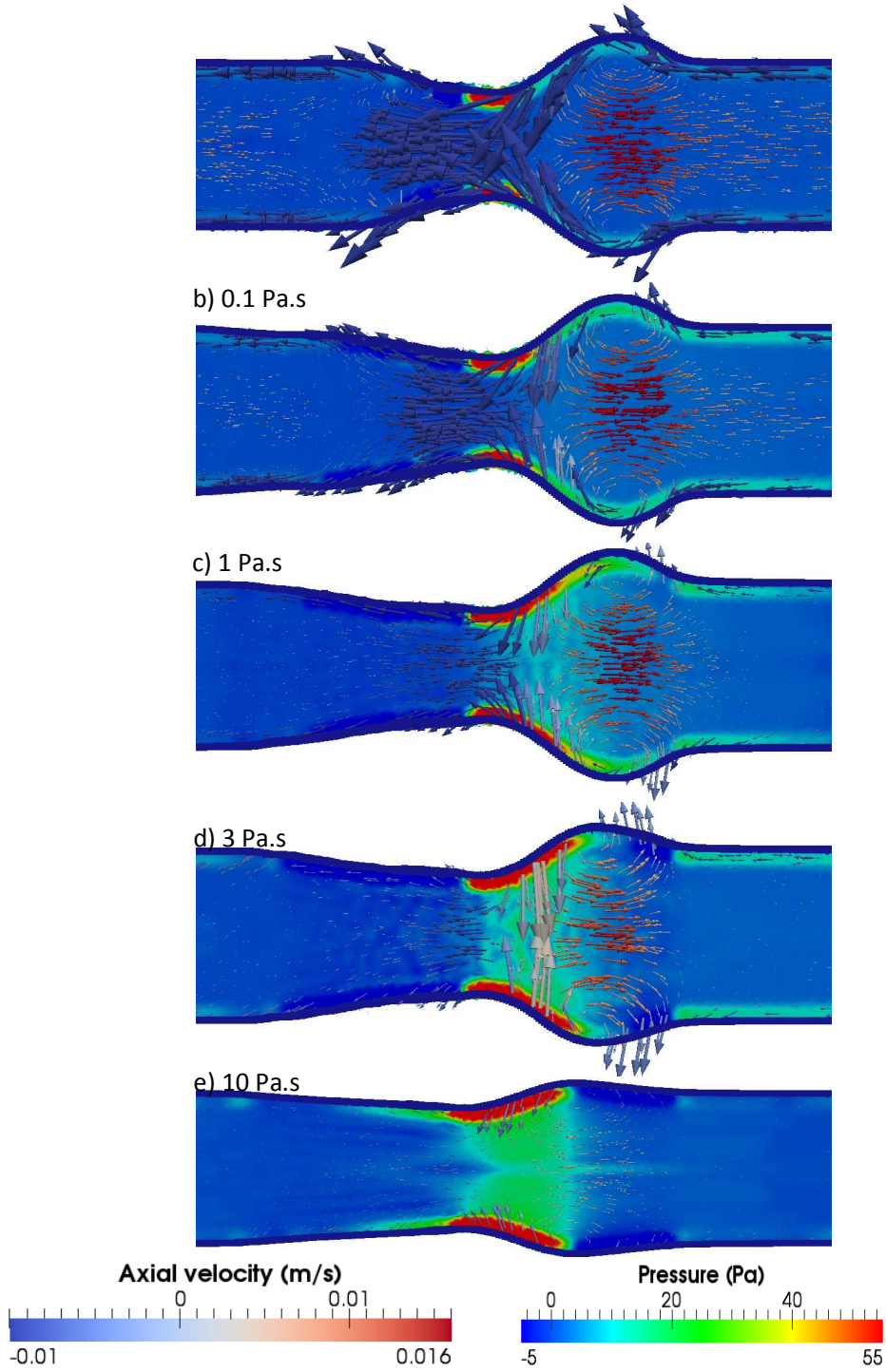


Figure 4: Vertical slice through the centre of the lumen with fluid color-shaded from blue to red by pressure for five different viscosities: a) 0.01; b) 0.1; c) 1.0; d) 3.0; e) 10 Pa s. Velocity arrows are colored by longitudinal speed for antegrade (red) and retrograde (blue) flow.

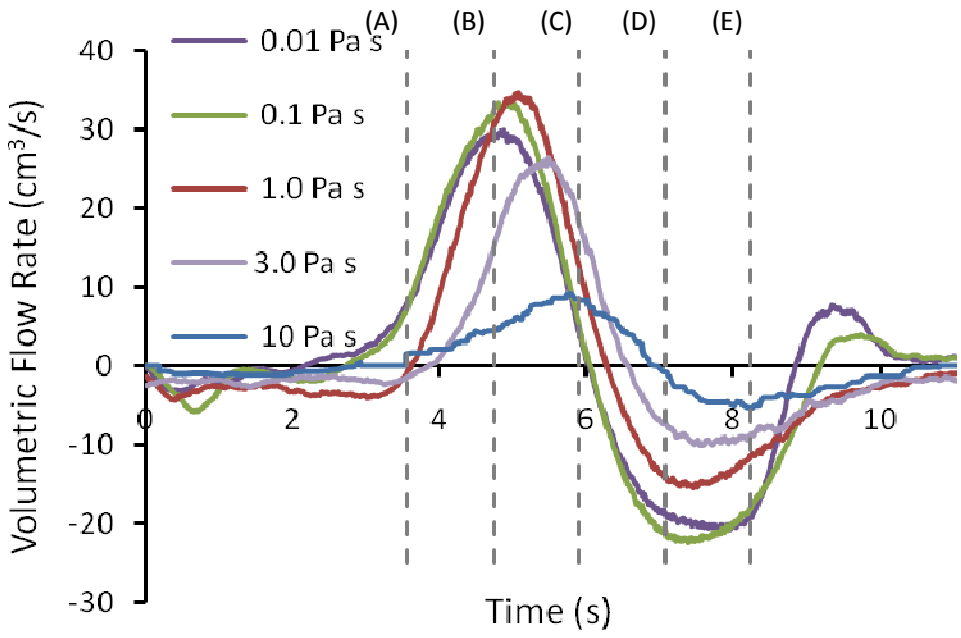


Figure 5: Time-variation of volumetric flow rates at a single longitudinal position for four viscosities. The vertical lines represent: (A) start of DI; (B) peak DI; (C) neutral part of the wave between DI and contraction; (D) peak contraction; and (E) end of the wave.

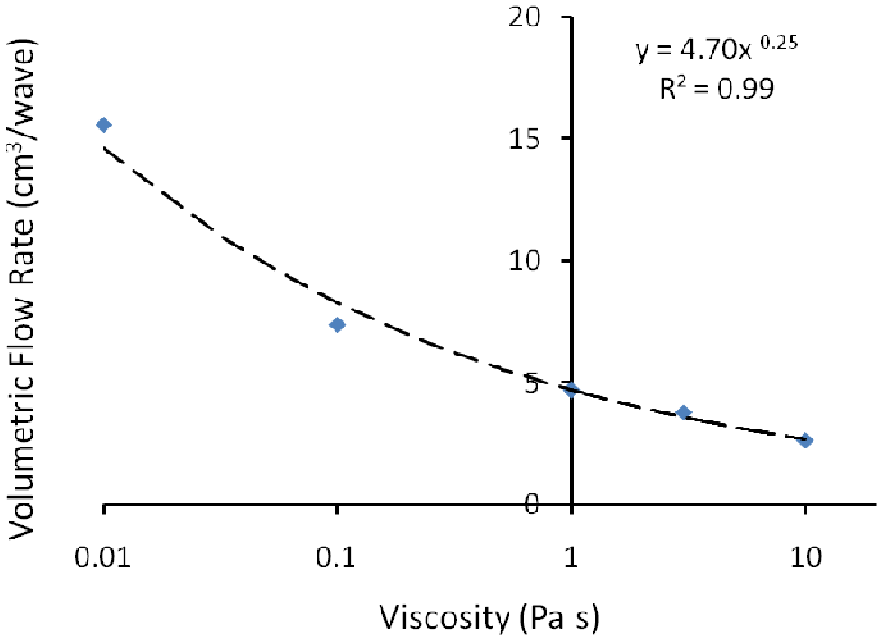


Figure 6: The relationship between net transport rate and fluid viscosity. An inverse power law fit to the measured flow rates (blue diamonds) is shown as the dashed line.

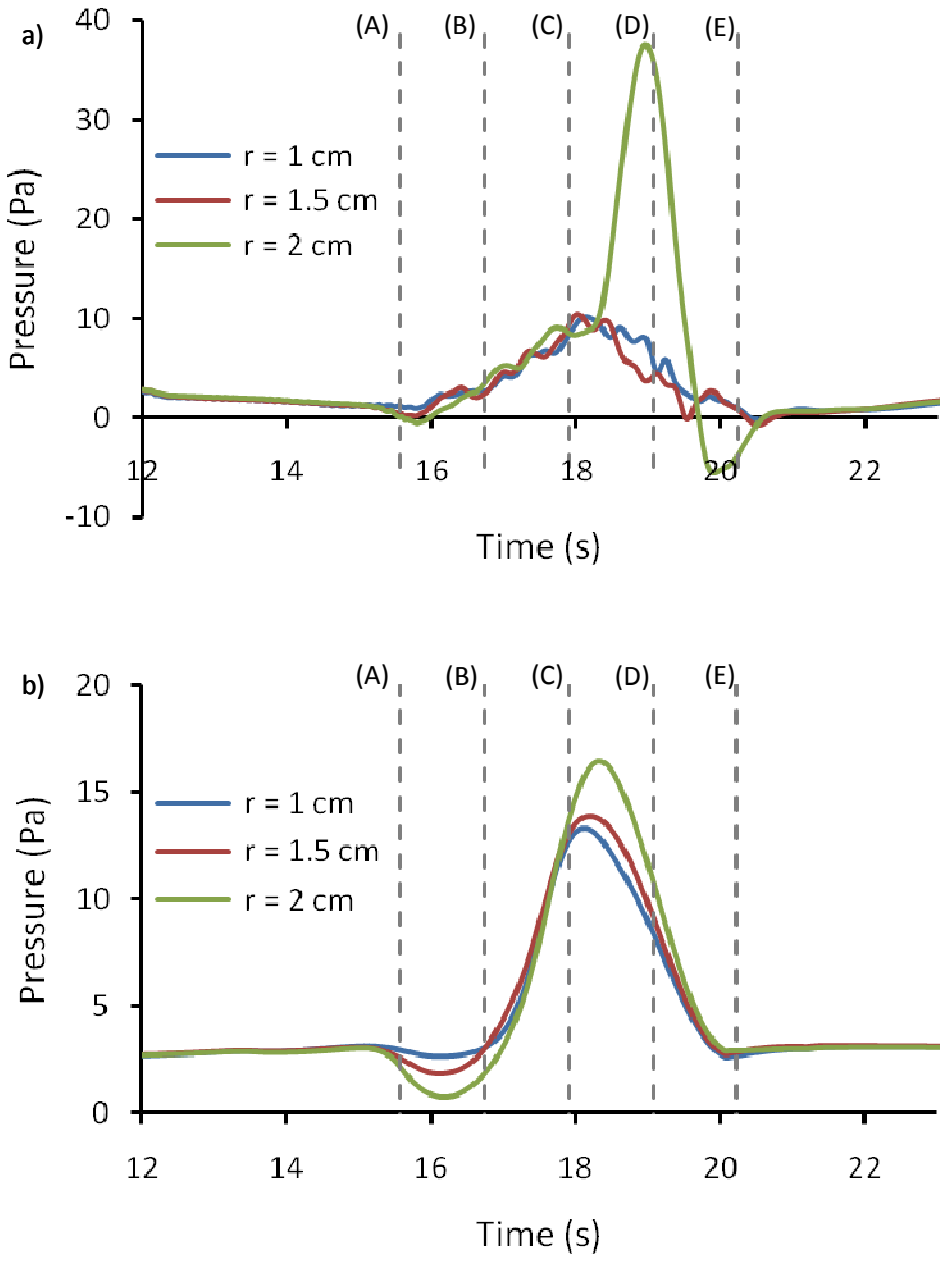


Figure 7: Pressure at radial distances of r = 1 (blue), 1.5 (red) and 2 cm (green) from the centre of the colon for viscosities: a) 1 Pa s, and b) 10 Pa s. The vertical lines represent: (A) start of DI; (B) peak DI; (C) neutral part of the wave between DI and contraction; (D) peak contraction; and (E) end of the wave.

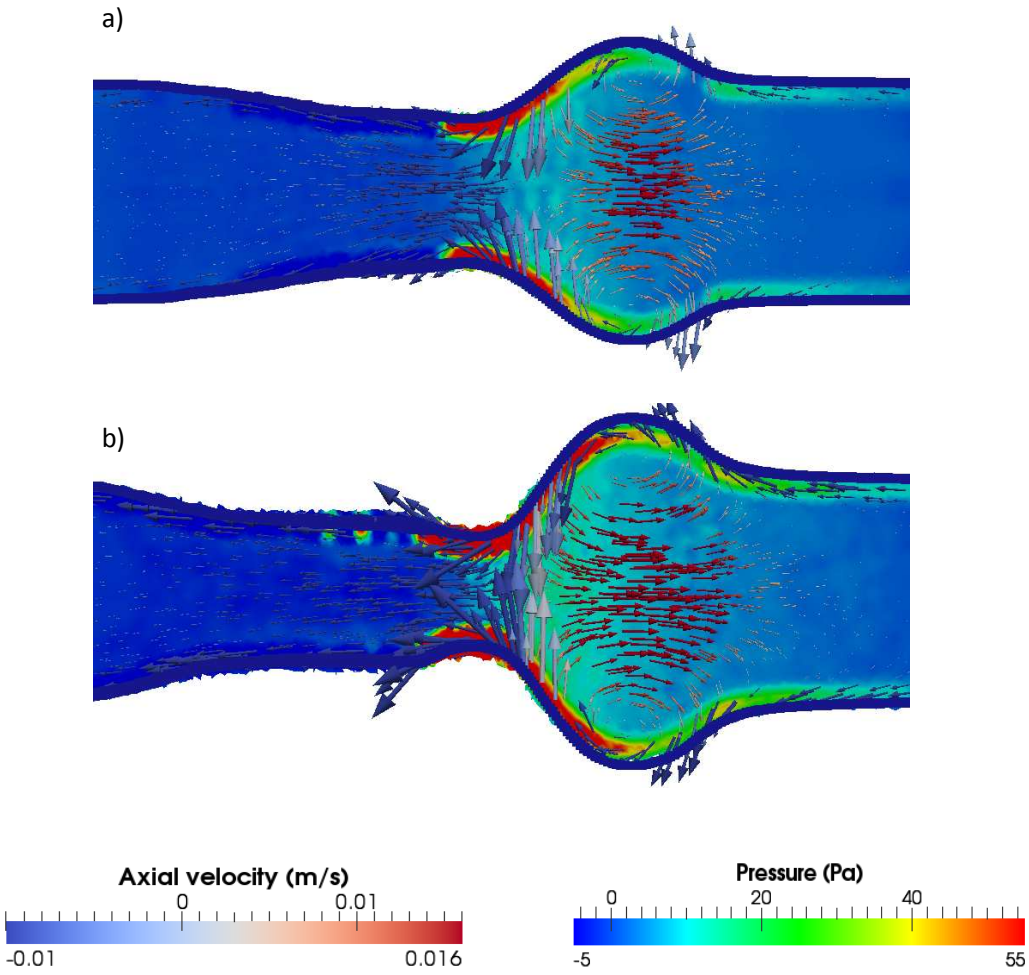


Figure 8: Vertical slice through the centre of the lumen with fluid color-shaded from blue to red by pressure for degrees of occlusion of a) 40%, and b) 80%. Velocity arrows are colored by longitudinal speed for antegrade (red) and retrograde (blue) flow.

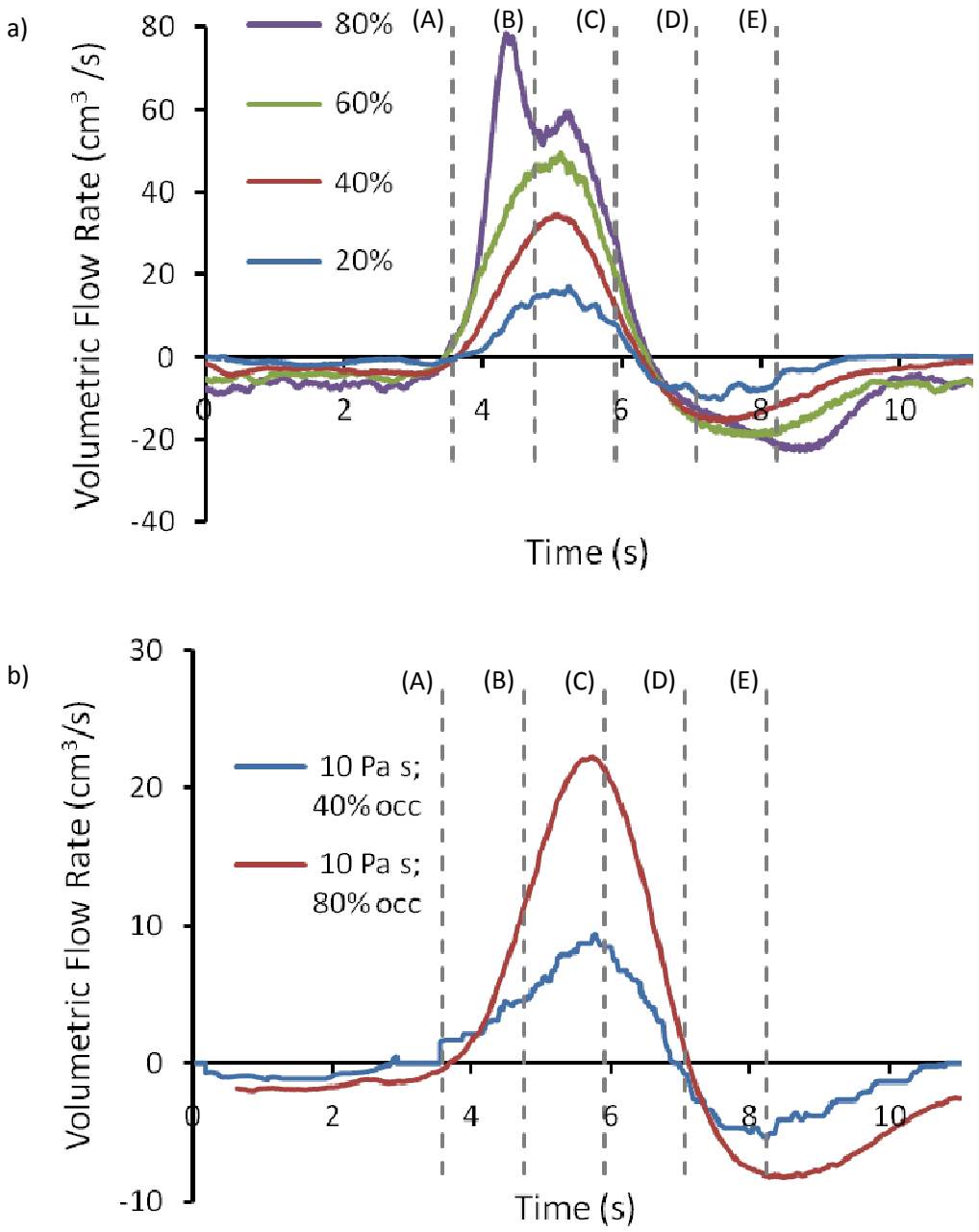


Figure 9: Time-variation of the volumetric flow rates at a single longitudinal position for different degrees of occlusion with viscosity: a) 1 Pa.s, and b) 10 Pa.s. The vertical lines represent: (A) start of DI; (B) peak DI; (C) neutral part of the wave between DI and contraction; (D) peak contraction; and (E) end of the wave.

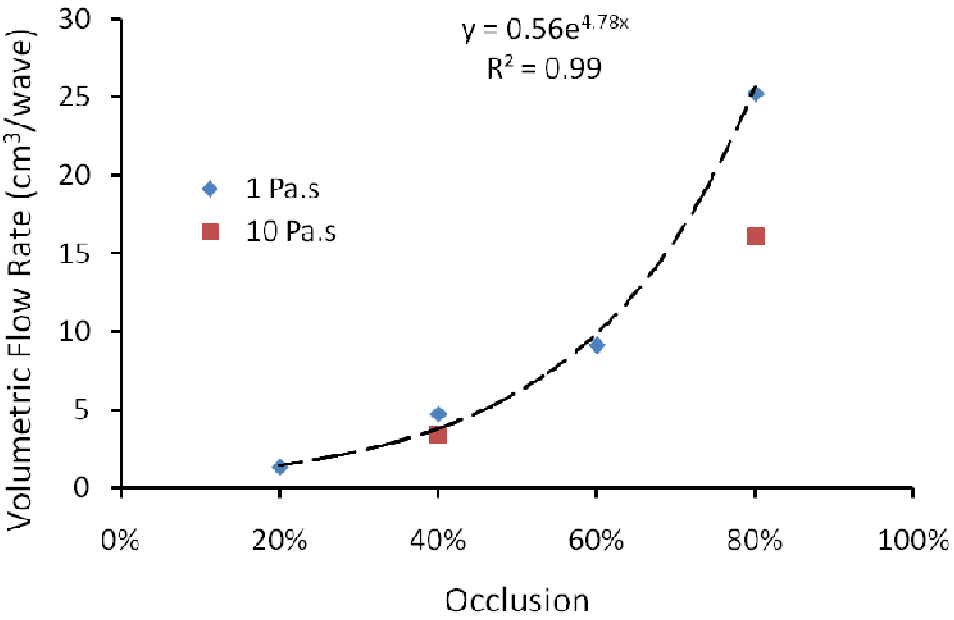


Figure 10: The relationship between degree of occlusion and resulting net flow rate considered for two viscosities (1 Pa.s and 10 Pa.s). An exponential fit to the 1 Pa.s data is shown as the dashed line.

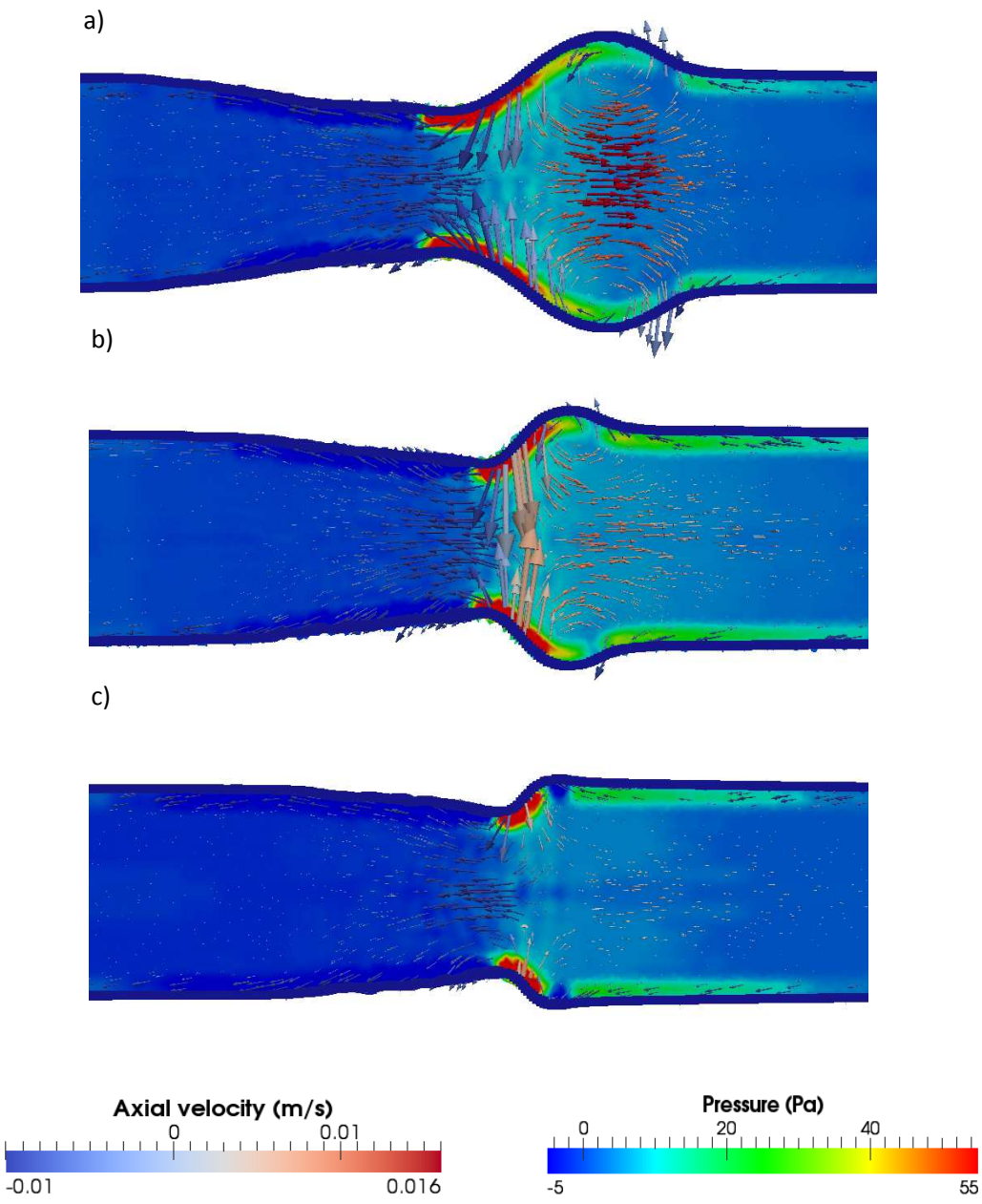


Figure 11: Vertical slice through the centre of the lumen with fluid color-shaded from blue to red by pressure for three different lengths of peristaltic wave: a) 8 cm; b) 4 cm; c) 2 cm. Velocity arrows are colored by longitudinal speed for antegrade (red) and retrograde (blue) flow.

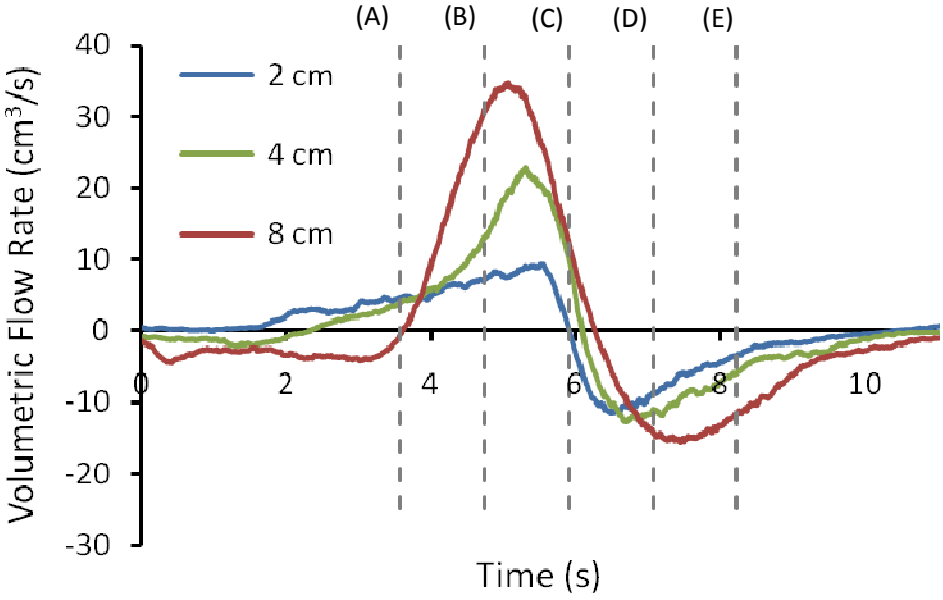


Figure 12: Time-variation of the mass flow rates at a single longitudinal position for peristaltic wave lengths of 2, 4 and 8 cm. The vertical lines represent: (A) start of DI; (B) peak DI; (C) neutral part of the wave between DI and contraction; (D) peak contraction; and (E) end of the wave.